J. Fluid Mech. (2014), *vol.* 753, *pp.* 131–149. © Cambridge University Press 2014
doi:10.1017/jfm.2014.351

Shear-imposed falling film

Arghya Samanta†

Department of Chemical Engineering, Indian Institute of Science, Bangalore, Karnataka 560012, India

(Received 19 December 2013; revised 5 June 2014; accepted 16 June 2014;
first published online 21 July 2014)

The study of a film falling down an inclined plane is revisited in the presence of imposed shear stress. Earlier studies regarding this topic (Smith, *J. Fluid Mech.*, vol. 217, 1990, pp. 469–485; Wei, *Phys. Fluids*, vol. 17, 2005*a*, 012103), developed on the basis of a low Reynolds number, are extended up to moderate values of the Reynolds number. The mechanism of the primary instability is provided under the framework of a two-wave structure, which is normally a combination of kinematic and dynamic waves. In general, the primary instability appears when the kinematic wave speed exceeds the speed of dynamic waves. An equality criterion between their speeds yields the neutral stability condition. Similarly, it is revealed that the nonlinear travelling wave solutions also depend on the kinematic and dynamic wave speeds, and an equality criterion between the speeds leads to an analytical expression for the speed of a family of travelling waves as a function of the Froude number. This new analytical result is compared with numerical prediction, and an excellent agreement is achieved. Direct numerical simulations of the low-dimensional model have been performed in order to analyse the spatiotemporal behaviour of nonlinear waves by applying a constant shear stress in the upstream and downstream directions. It is noticed that the presence of imposed shear stress in the upstream (downstream) direction makes the evolution of spatially growing waves weaker (stronger).

Key words: low-dimensional models, nonlinear dynamical systems, transition to turbulence

1. Introduction

Studies of wave dynamics on the surface of a falling film are still a fascinating topic, and interest in such problems seems to be attracting more attention since Kapitza (1948), because of the prevalence of such films in chemical and technological processes. It has already been established that the surface waves may change the heat and mass transfer rates significantly in process equipment (Brauner & Maron 1982). In addition, the formation of a wave on the surface of a coating film degrades the quality of the final product and, indeed, plays a crucial role in coating technology (Weinstein & Ruschak 2004). Further, there is already experimental evidence (Alekseenko, Nakoryakov & Pokusaev 1985; Liu, Paul & Gollub 1993; Liu & Gollub 1994) that an infinitesimal disturbance on the surface of a falling film evolves slowly downstream through a sequence of nonlinear events until solitary waves are formed. The development of such a wave phenomenon is only possible when the Reynolds

† Present address: Linné FLOW Centre, KTH Mechanics, SE-100 44 Stockholm, Sweden.
Email address for correspondence: arghyar@gmail.com

https://doi.org/10.1017/jfm.2014.351 Published online by Cambridge University Press

number exceeds a critical value, which was theoretically predicted by Benjamin (1957) and Yih (1963) and experimentally confirmed by Liu *et al.* (1993). Although the derivation of a critical Reynolds number based on the long-wave expansion is quite simple, the study of the mechanism of instability always remains an essential part of the problem.

The mechanism of the primary instability on the surface of a film falling down an inclined plane was initiated by Kelley *et al.* (1989) using the energy budget method. According to their study, the instability begins at sufficiently long wavelength through the increase of the kinetic energy of an infinitesimal disturbance with time. An alternative discussion regarding the mechanism of a falling film instability in the presence of imposed shear stress was provided by Smith (1990). He reported that the unsteadiness associated with perturbation of a base flow is the dominant cause of a long-wave instability. Later, Wei (2005*a*) extended this study by including an insoluble surfactant at the top of a film surface. In general, a surfactant exhibits a stabilizing effect on a surface wave by suppressing the long-wave instability. However, the presence of both constant shear stress and insoluble surfactant may cause a shear-induced Marangoni instability (Wei 2007).

In this article, our purpose is to extend the study of Smith (1990) up to moderate values of the Reynolds number based on the low-dimensional model, which is normally a coupled system of two evolution equations for local film thickness $h(x, t)$ and local flow rate $q(x, t)$. An alternative instability mechanism is provided under the framework of kinematic and dynamic waves, where the instability originates when the kinematic wave speed overtakes the speed of dynamic waves. It is demonstrated that the presence of imposed shear stress intensifies the primary instability. However, an increasing magnitude of imposed shear stress shows opposite behaviour, i.e. a stabilizing effect on the primary instability. In the nonlinear regime, it is further elucidated that the travelling wave solutions also depend on the kinematic and dynamic wave speeds. The equality criterion between their speeds leads to an analytical expression for the speed of a family of travelling wave solutions as a function of the Froude number. In addition, this analytical expression recovers the critical Froude number for the primary instability exactly at the primary neutral wave speed. This result demonstrates a connection between the primary neutral wave and secondary travelling wave solutions. Direct numerical simulations (DNS) of the low-dimensional model predict that the action of imposed shear stress in the downstream direction strengthens the transition process from small-amplitude sinusoidal waves to finite-amplitude localized pulses with a big hump preceded by capillary ripples. On the other hand, it weakens the evolution of spatially growing waves if the imposed shear stress acts in the upstream direction.

2. Governing equations

Consider the flow of a gravity-driven viscous incompressible liquid film down an inclined plane in the presence of a constant shear stress τ_s, acting parallel to the plane at the free surface, as sketched in figure 1. The negative and positive values of τ_s, respectively, imply the action of shear stress in the upstream and downstream directions. Assume that the physical properties of the liquid, such as density ρ, dynamic viscosity μ, surface tension σ and inclination angle θ, are constants. The origin is located at the plane and the coordinate axes x and y are placed along

https://doi.org/10.1017/jfm.2014.351 Published online by Cambridge University Press

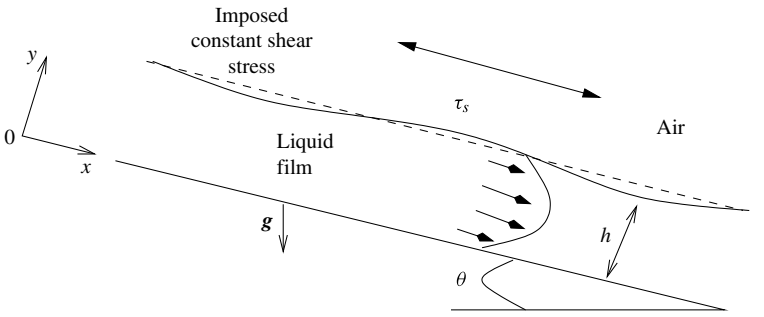


FIGURE 1. Schematic diagram of a shear-imposed film flow.

the streamwise and crosswise flow directions, respectively. The governing equations corresponding to the flow are

$$\boldsymbol{\nabla}\cdot\boldsymbol{v}=0, \tag{2.1a}$$

$$\rho\frac{\mathrm{D}\boldsymbol{v}}{\mathrm{D}t}=-\boldsymbol{\nabla}p+\mu\nabla^2\boldsymbol{v}+\rho\boldsymbol{g}, \tag{2.1b}$$

where $\boldsymbol{v}=(u,\ v)$ and p are, respectively, the velocity vector and pressure of a liquid film, and $\boldsymbol{g}=(g\sin\theta,\ -g\cos\theta)$ is the gravitational acceleration. The flow system is subject to the following boundary conditions. (i) At the plane $y=0$, the no-slip and no-penetration conditions lead to

$$\boldsymbol{v}=0. \tag{2.1c}$$

(ii) At the free surface $y=h(x,\ t)$, the tangential stress is balanced by the imposed shear stress, whereas the normal stress is balanced by surface tension times curvature and yields the dynamic condition (Smith 1982, 1990; Wei 2005*a*,*b*, 2007)

$$\boldsymbol{T}\cdot\boldsymbol{n}+\sigma(\boldsymbol{\nabla}\cdot\boldsymbol{n})\boldsymbol{n}-\tau_s\boldsymbol{t}=0, \tag{2.1d}$$

where $\boldsymbol{T}$ is the stress tensor, $\boldsymbol{n}$ is the unit normal and $\boldsymbol{t}$ is the unit tangent vector. Without loss of generality, we neglect the atmospheric pressure p_{atm}. (iii) In addition, the kinematics of the liquid film surface is described by

$$\frac{\mathrm{D}}{\mathrm{D}t}[y-h(x,\ t)]=0, \tag{2.1e}$$

where $\mathrm{D}/\mathrm{D}t=(\partial_t+\boldsymbol{v}\cdot\boldsymbol{\nabla})$ is the substantial derivative. Here, the uniform Nusselt film thickness h_N is chosen as length scale, while the velocity scale $V=\rho g\sin\theta\,h_N^2/\mu$ is defined from the balance of the viscous friction force per unit volume, $\propto\mu V/h_N^2$, and the streamwise gravity force per unit volume, $\propto\rho g\sin\theta$. The time and pressure scales are chosen as h_N/V and $\mu V/h_N$, respectively. According to this scaling, the dimensionless base flow solution with a uniform liquid layer thickness $y=1$ is determined and expressed as

$$U(y)=(1+\tau)y-y^2/2,\quad y\in[0,\ 1], \tag{2.1f}$$

$$V(y)=0, \tag{2.1g}$$

$$P(y)=\cot\theta\,(1-y), \tag{2.1h}$$

where $\tau=\bar{\tau}_s h_N/(\mu V)$ is the dimensionless magnitude of the imposed shear stress and $\bar{\tau}_s$ is the dimensional magnitude of the imposed shear stress.

https://doi.org/10.1017/jfm.2014.351 Published online by Cambridge University Press

3. Low-dimensional model

The complete Navier–Stokes (NS) equations for a free surface flow are difficult to tackle except numerically (Salamon, Armstrong & Brown 1994; Ramaswamy, Chippada & Joo 1996; Malamataris, Vlachogiannis & Bontozoglou 2002; Gao, Morley & Dhir 2003). Instead, the simplification of the NS equations is more suitable and can be accomplished using the boundary layer approximation together with the depth-averaged method (Shkadov 1967; Chang, Demekhin & Kopelvitch 1993; Chang 1994; Nguyen & Balakotaiah 2000; Ruyer-Quil & Manneville 2000). The reduced equations normally consist of a coupled system of two equations in terms of local film thickness $h(x, t)$ and local flow rate $q(x, t)$. The motivation is to extend the previous model, studied by Smith (1990) and Wei (2005*a*), in detail up to moderate values of the Reynolds number when the free surface is uncontaminated. We propose a two-equation model that is consistent up to order $O(\epsilon)$ in inertial terms and up to order $O(\epsilon^2)$ in viscous diffusion terms, where $\epsilon \sim (1/\lambda) \ll 1$ and the wavelength λ of the disturbance is large compared to the depth of the liquid film. We assume that the free surface evolves slowly downstream with respect to space and time, and this fact is a measure of the order of differentiation of different flow variables, i.e. $\partial_x = O(\epsilon)$ and $\partial_t = O(\epsilon)$. Based on this approximation, the dimensionless NS equations and the associated boundary conditions are greatly simplified and can be rewritten consistent up to order $O(\epsilon^2)$ as

$$\partial_x u + \partial_y v = 0, \tag{3.1a}$$

$$Re(\partial_t u + u\partial_x u + v\partial_y u) + \partial_x p - \partial_{xx} u - \partial_{yy} u - 1 = 0, \tag{3.1b}$$

$$\partial_y p - \partial_{yy} v + \cot\theta = 0, \tag{3.1c}$$

$$u|_0 = v|_0 = 0, \tag{3.1d}$$

$$(\partial_y u + \partial_x v)|_h - 4\partial_x u \partial_x h|_h - \tau(1 + \tfrac{3}{2}\partial_x h^2) = 0, \tag{3.1e}$$

$$p|_h - 2\partial_y v|_h + We\partial_{xx} h + 2\tau\partial_x h = 0, \tag{3.1f}$$

where $Re = \rho V h_N/\mu$ is the Reynolds number, $We = \sigma/\mu V = \Gamma/Re^{2/3}$ is the Weber number and $(x, y, t) \in \mathbb{R} \times [0, h] \times [0, \infty)$. Here $\Gamma = \sigma\rho^{1/3}/[\mu^{4/3}(g\sin\theta)^{1/3}]$ is the Kapitza number, which is often used because of its dependence on only the physical properties of the liquid. The term $We\partial_{xx}h$ is kept in the normal stress balance on account of the higher magnitude of surface tension ($We = O(\epsilon^{-2})$), the stabilizing influence of which assists in preventing the breakup of nonlinear wave phenomenon. It can be found that the y momentum equation and related boundary condition are retained up to $O(\epsilon)$ in order to eliminate the streamwise pressure gradient term $\partial_x p$ in the x momentum equation (3.1*b*), which is itself of $O(\epsilon)$. Integration of the y momentum equation (3.1*c*) and use of the normal stress boundary condition (3.1*f*) lead to the following expression for the pressure distribution:

$$p(x, y, t) = -\partial_x u - \partial_x u|_h + \cot\theta\,(h - y) - We\partial_{xx} h - 2\tau\partial_x h. \tag{3.2}$$

Similarly, integration of the continuity equation (2.1*a*) over the depth of the liquid film $[0, h]$ and use of the kinematic boundary condition (2.1*e*) yield the averaged mass conservation equation

$$\partial_t h + \partial_x q = 0, \tag{3.3}$$

where $q(x, t) = \int_0^h u\,\mathrm{d}y$ is the local flow rate of the liquid film. For convenience, the crosswise velocity component v is replaced in terms of the streamwise velocity

https://doi.org/10.1017/jfm.2014.351 Published online by Cambridge University Press

component u as

$$v(x, y, t) = -\int_0^y \partial_x u \, \mathrm{d}y = O(\epsilon), \quad y \in [0, h]. \tag{3.4}$$

Substituting the pressure distribution (3.2) in the x momentum equation (3.1b), one can obtain

$$Re(\partial_t u + u\partial_x u + v\partial_y u) = 1 - \cot\theta\, \partial_x h + We\partial_{xxx} h + \partial_{yy} u + 2\partial_{xx} u + \partial_x[\partial_x u|_h] + 2\tau\partial_{xx} h. \tag{3.5}$$

Note that in (3.5) the explicit expression for the streamwise velocity distribution $u(x, y, t)$ is necessary to complete the averaged momentum equation. To do this, the approach proposed by Ruyer-Quil & Manneville (2000), Samanta, Ruyer-Quil & Goyeau (2011), Samanta (2013a) and Samanta, Goyeau & Ruyer-Quil (2013) is used systematically. Following Samanta (2013a), suppose that $u = u_0 + u_1$, where

$$u_0(x, y, t) = a(x, t)y^2 + b(x, t)y + c(x, t), \quad y \in [0, h], \tag{3.6}$$

satisfies the base flow configuration, i.e. $u_0|_0 = 0$, $\partial_y u_0|_h = \tau$ and $\int_0^h u_0 \, \mathrm{d}y = q$, which leads to

$$a(x, t) = \frac{3h^2\tau - 6q}{4h^3}, \quad b(x, t) = \frac{6q - h^2\tau}{2h^2}, \quad c(x, t) = 0. \tag{3.7a–c}$$

Here u_1 is a correction of leading-order velocity u_0 and it is considered to capture the deformation of the free surface. Moreover, u_1 must satisfy $\int_0^h u_1 \, \mathrm{d}y = 0$ to ensure the total flow rate q of the entire system. However, the evaluation of u_1 is not necessary in the subsequent calculation. Rather, the weight function $w(x, y, t)$ is recalled to implement the weighted residual approach (Finlayson 1972), where the weight function $w(x, y, t)$ must satisfy

$$\partial_{yy} w = d_2, \quad w|_0 = 0, \quad \partial_y w|_h = 0, \quad y \in [0, h]. \tag{3.8a–d}$$

Here d_2 is an arbitrary constant. Multiplying the weight function w with (3.5) and integrating over the film depth $[0, h]$, we are able to derive the following averaged momentum conservation equation:

$$\begin{aligned} &Re[\partial_t q + \tfrac{17}{7} q\partial_x q/h - \tfrac{9}{7} q^2/h^2 \partial_x h] \\ &\quad = \tfrac{5}{6} h(1 - \cot\theta\, \partial_x h + We\partial_{xxx} h) - \tfrac{5}{2} q/h^2 \\ &\qquad + [4q/h^2 \partial_x h^2 - \tfrac{9}{2}\partial_x q \partial_x h/h - 6q/h\partial_{xx} h + \tfrac{9}{2}\partial_{xx} q] + \tau[\tfrac{5}{4} - \tfrac{5}{112} Req\partial_x h \\ &\qquad - \tfrac{19}{336} Reh\partial_x q - \tfrac{1}{8}(\partial_x h)^2 + \tfrac{1}{6} h\partial_{xx} h] - \tfrac{19}{672} Re\tau^2 h^2 \partial_x h. \end{aligned} \tag{3.9}$$

Equations (3.3) and (3.9) constitute a two-equation model for a shear-imposed falling film and the model is valid up to $O(\epsilon)$ in inertial terms and valid up to $O(\epsilon^2)$ in viscous diffusion terms. The present model recovers exactly the same two-equation model as derived by Ruyer-Quil & Manneville (2000) in the limit $\tau \to 0$, i.e. when the imposed shear stress is absent at the free surface.

4. Linear temporal stability

The linear stability of the low-dimensional model (3.3) and (3.9) is performed by using the normal mode decomposition, where an infinitesimal perturbation is

https://doi.org/10.1017/jfm.2014.351 Published online by Cambridge University Press

considered from a uniform parallel solution $h=1$. Accordingly, let us assume that

$$h(x,t)=1+h_1\exp[\mathrm{i}k(x-ct)],\quad (x,t)\in\mathbb{R}\times[0,\infty), \tag{4.1}$$

$$q(x,t)=q_0+q_1\exp[\mathrm{i}k(x-ct)], \tag{4.2}$$

where $q_0=\int_0^1 U(y)\,\mathrm{d}y=(1/3+\tau/2)$ is the dimensionless flow rate at the base state, where $U(y)$ is given in (2.1*f*). Here $k\in\mathbb{R}$ and $c\in\mathbb{C}$ are, respectively, the wavenumber and wave speed of the disturbance. Inserting the expressions for h and q in the two-equation model (3.3) and (3.9) and linearizing with respect to the uniform solution $h=1$, we obtain a quadratic polynomial in c:

$$\mathrm{i}(c-c_k)+\Omega(Re)k(c-c_{d+})(c-c_{d-})=0, \tag{4.3}$$

where

$$c_k=[1+\tfrac{4}{5}k^2+\tau(1+\tfrac{17}{15}k^2)]/(1+\tfrac{9}{5}k^2), \tag{4.4}$$

$$c_{d\pm}=\frac{17}{42}+\frac{61}{96}\tau\pm\sqrt{\frac{37}{1764}+\frac{5\cot\theta}{6Re}+\frac{5k^2We}{6Re}+\frac{29}{288}\tau+\frac{1225}{9216}\tau^2} \tag{4.5}$$

and $\Omega(Re)=2Re/(5+9k^2)$. The dispersion relation (4.3) can also be expressed as a composition of two linear hyperbolic waves,

$$(\partial_t+c_k\partial_x)h+\Omega(Re)(\partial_t+c_{d+}\partial_x)(\partial_t+c_{d-}\partial_x)h=0. \tag{4.6}$$

The lower-order wave equation $(\partial_t+c_k\partial_x)h$ depends primarily on the mass conservation equation (3.3) and, for this reason, this wave is given the name 'kinematic wave', which propagates with a speed $c_k=(\mathrm{d}q/\mathrm{d}h)|_{h=1}$ at $k\to 0$. On the other hand, the higher-order wave equation $(\partial_t+c_{d+}\partial_x)(\partial_t+c_{d-}\partial_x)h$ is basically developed by depthwise gravitational force and inertia force where surface tension plays the role of dispersion and consequently these waves are referred to as 'dynamic waves'. Moreover, these dynamic waves propagate with speeds $c_{d\pm}$ respectively. Using long-wave expansion ($k\to 0$), one can easily reduce (4.3) to the following form:

$$c=c_k+\mathrm{i}k\Omega(Re)(c_k-c_{d-})(c_k-c_{d+})+O(k^2). \tag{4.7}$$

The interesting feature is that the primary instability will damp to long-wave disturbances if the following criterion is satisfied:

$$c_{d-}<c_k<c_{d+}. \tag{4.8}$$

Thus one can infer that the surface wave instability fully relies on the competition between kinematic and dynamic waves. An infinitesimal disturbance will grow with time if the kinematic wave speed c_k exceeds the speed of dynamic wave c_{d+}; otherwise it will damp. Such an alternative primary instability mechanism was initiated by Whitham (1974), Alekseenko *et al.* (1985) and Kalliadasis *et al.* (2012) in the context of a shallow water model. The equality condition $c_k=c_{d+}$ leads to

$$Re=\frac{1}{(1+\tau)}\frac{5\cot\theta}{2}+k^2\frac{1}{(1+\tau)^2}\left(\frac{125}{14}\cot\theta+\frac{5}{2}We+\frac{7675}{672}\cot\theta\,\tau+\frac{5}{2}We\tau+\frac{175}{48}\cot\theta\,\tau^2\right)+O(k^4), \tag{4.9}$$

https://doi.org/10.1017/jfm.2014.351 Published online by Cambridge University Press

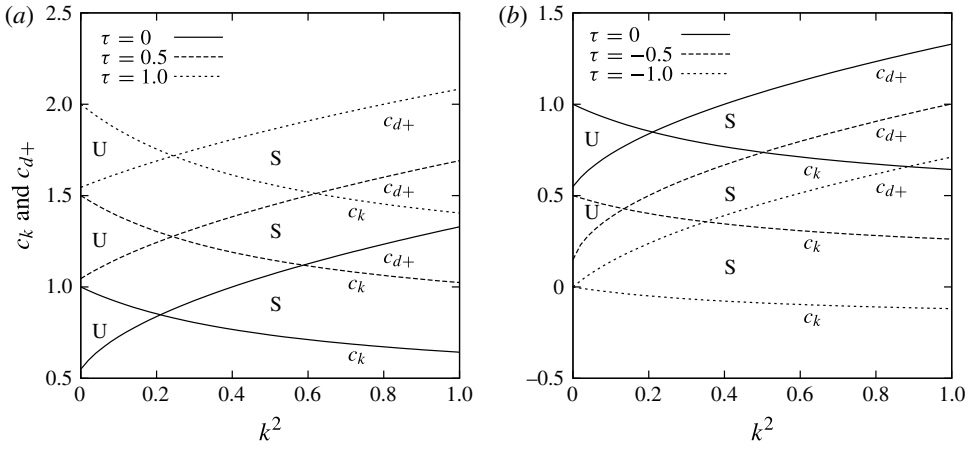


FIGURE 2. The variation of kinematic and dynamic wave speeds as a function of k^2 when the imposed shear stress varies successively in the upstream and downstream directions. Here $Re = We = 1$ and $\theta = 90°$. The symbols 'U' and 'S' respectively represent the unstable and stable regions.

which recovers the critical Reynolds number very well for a shear-imposed falling film $Re_c = 5\cot\theta/[2(1+\tau)]$, obtained by Smith (1990) and Wei (2005*a*) in the limit $k \to 0$, i.e. when the streamwise viscous dissipation terms are ignored into the model. Equation (4.9) can be rewritten in terms of the Froude number as

$$Fr^2 = \frac{1}{(1+\tau)}\frac{5}{2} + k^2\frac{1}{(1+\tau)^2}\left(\frac{125}{14} + \frac{5}{2}\frac{We}{\cot\theta} + \frac{7675}{672}\tau + \frac{5}{2}\frac{We}{\cot\theta}\tau + \frac{175}{48}\tau^2\right) + O(k^4), \tag{4.10}$$

where $Fr^2 = Re/\cot\theta$ and $Fr_c^2 = 5/[2(1+\tau)]$. Note that the critical Reynolds number, or equivalently the critical Froude number, is sensitive to the imposed shear stress. The variation of speed corresponding to the kinematic and dynamic waves with the imposed shear stress is illustrated in figure 2. Let us first consider the case of the vertical limit, i.e. $\theta = 90°$. In this limit, if the imposed shear stress acts in the downstream direction, i.e. $\tau > 0$, the kinematic wave speed, which is faster initially than the dynamic wave speed, increases with the shear stress but decreases continuously with the square of the wavenumber. On the other hand, the dynamic wave speed c_{d+} accelerates with the shear stress as well as enhancing with the square of the wavenumber and eventually overtakes the speed of the kinematic wave, and this fact leads to a stabilizing effect. It is noted that the unstable region increases in the presence of imposed shear stress. If the imposed shear stress acts in the upstream direction, i.e. $\tau < 0$, the kinematic wave speed, which is faster initially than the dynamic wave speed, decelerates with the shear stress as well as decaying continuously with the square of the wavenumber. On the other hand, the dynamic wave speed c_{d+} decelerates in the presence of imposed shear stress but enhances continuously with the square of the wavenumber and eventually overtakes the speed of the kinematic wave, and this fact leads to a stabilizing effect. In this case, the unstable region decreases in the presence of imposed shear stress. It can be found that there exists a situation where the unstable region is no longer observable (see figure 2*b*).

https://doi.org/10.1017/jfm.2014.351 Published online by Cambridge University Press

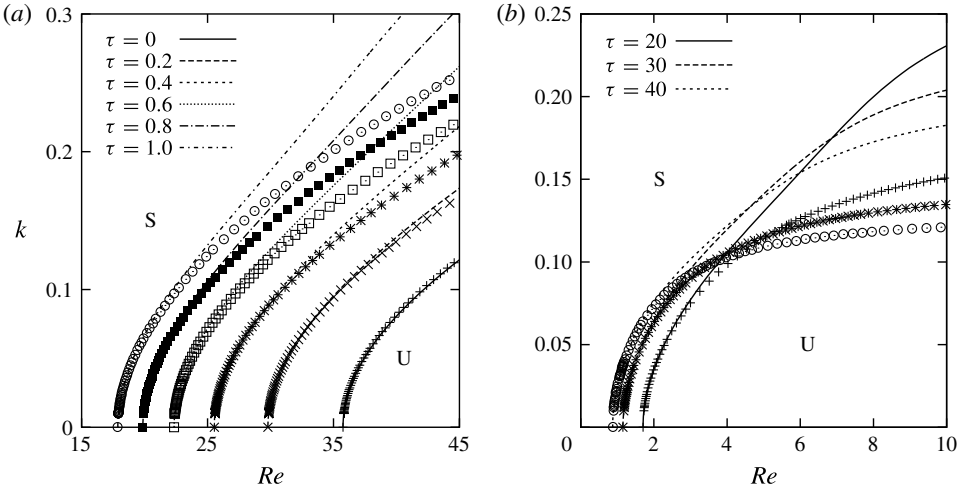


FIGURE 3. The variation of marginal stability curves in the (Re, k) plane when the shear stress varies successively in the downstream direction. Here $\theta = 4^\circ$ and $\Gamma = 2341.0$. The lines represent the result corresponding to the OS BVP and the points are the result of the low-dimensional model (3.3) and (3.9). The symbols 'U' and 'S' respectively represent the unstable and stable regions.

4.1. *Comparison with Orr–Sommerfeld boundary value problem*

In this section, we check the validity of the low-dimensional model (3.3) and (3.9) by comparing the results with those of the Orr–Sommerfeld boundary value problem (OS BVP) (Smith 1990; Wei 2005*a*). The associated marginal curves are produced up to moderate values of the Reynolds number for a glycerine–water mixture with kinematic viscosity $\mu/\rho = 2.3 \times 10^{-6}$ m^2 s^{-1} and $\sigma/\rho = 62.6 \times 10^{-6}$ m^3 s^{-2} (Samanta *et al.* 2011; Samanta 2013*b*) by applying a constant shear stress in the downstream direction. The ensuing results can be found in figure 3. It is noticed that the primary instability is destabilizing in the presence of imposed shear stress and this fact is consistent with the result in figure 2(*a*). However, with an increasing magnitude of shear stress, the unstable region reduces when the Reynolds number lies far from the threshold of instability. Physically, there is a competition between the inertial force and the normal stress induced by the imposed shear stress, equal to $2\tau\partial_x h$, which can be found in the pressure distribution (3.2). When the magnitude of shear stress is quite low, the base flow velocity distribution, or equivalently the base flow rate, accelerates with the imposed shear stress. This fact triggers the inertia force, which dominates over the normal stress induced by the imposed shear stress and strengthens the primary instability close to the onset of instability. On the other hand, when the magnitude of the imposed shear stress is quite high, the normal stress induced by the imposed stress dominates over the inertial force far from the onset of instability and leads to a stabilizing influence on the primary instability.

5. Travelling wave solution

There is already experimental evidence that a falling film has the property of exhibiting travelling wave solutions that propagate with a constant speed and shape relative to the moving frame (Alekseenko *et al.* 1985; Liu *et al.* 1993; Liu & Gollub 1994). It is only possible to manifest such a wave downstream by controlling

https://doi.org/10.1017/jfm.2014.351 Published online by Cambridge University Press

the frequency of the inlet disturbance. Using the moving frame of transformation $\xi = x - ct$ and integrating the mass conservation equation (3.3) with respect to ξ, we obtain $q = q_0 + ch$, where c is the speed of the reference frame and q_0 is the flow rate under the wave. Similarly, the momentum conservation equation (3.9) can be transformed to the following form:

$$\begin{aligned} &Reh'[c^2 - \tfrac{17}{7}cq/h + \tfrac{9}{7}q^2/h^2] \\ &\quad = \tfrac{5}{2}q/h^2 - \tfrac{5}{6}h(1 - \cot\theta\, h' + Weh''') \\ &\qquad - [4q/h^2(h')^2 - \tfrac{9}{2}c/h(h')^2 - 6q/hh'' + \tfrac{9}{2}ch''] - \tau[\tfrac{5}{4} - \tfrac{5}{112}Reqh' \\ &\qquad - \tfrac{19}{336}Rechh' - \tfrac{1}{8}(h')^2 + \tfrac{1}{6}hh''] + \tfrac{19}{672}Re\tau^2h^2h', \end{aligned} \tag{5.1}$$

where the prime denotes the derivative with respect to ξ. Equation (5.1) is able to describe various types of travelling wave solutions, which are characterized by their humps. However, we restrict our attention to the solitary wave solutions whose front and back tails approach an asymptotic value for a flat film at infinity. In what follows, $h' = h'' = h''' = 0$ at $\xi \to \pm\infty$ and (5.1) simply reduces to a cubic equation in h:

$$q_0 = \tfrac{1}{3}h^3 + \tfrac{1}{2}\tau h^2 - ch. \tag{5.2}$$

The Nusselt film thickness $h_I = 1$ is itself a solution of (5.2). Thus, it must satisfy

$$q_0 = \tfrac{1}{3} + \tfrac{1}{2}\tau - c. \tag{5.3}$$

Solving (5.2) and (5.3), we obtain a second solution for a flat film

$$h_{II} = \tfrac{1}{4}\left(-2 - 3\tau + \sqrt{3}\sqrt{16c - 4 - 4\tau + 3\tau^2}\right). \tag{5.4}$$

Note that the second solution recovers the result of a gravity-driven film falling down an inclined plane very well when the imposed shear stress vanishes at the free surface (Ruyer-Quil & Manneville 2005; Samanta *et al.* 2011). It would be useful to discuss solutions of (5.1) in the framework of dynamical system theory. To do this, we recast (5.1) to a system of first-order ordinary differential equations (ODEs) of the form

$$\frac{\mathrm{d}U}{\mathrm{d}\xi} = \mathscr{F}(U), \quad \xi \in [-L, L], \tag{5.5}$$

where $U = (h, h', h'')^{\mathrm{T}}$ is a column matrix and $2L$ is the period of the travelling wave. Equation (5.5) is resolved numerically by using the continuation software AUTO 07p (Doedel *et al.* 2007). The results are produced corresponding to a glycerine–water mixture with Kapitza number $\Gamma = 253$ by applying an imposed shear stress in the downstream direction. In addition, we assume the vertical limit case, i.e. $\theta = 90°$. Figure 4 exposes wave profiles corresponding to the travelling wave for various magnitudes of imposed shear stress. It is noted that the maximum amplitude of the wave profile amplifies with rising values of shear stress, which agrees satisfactorily with the results of primary instability when the imposed shear stress lies in the range [0, 1.2], i.e. the presence of imposed shear stress intensifies the transition process from primary flow to secondary flow. However, the rate of increment of the maximum amplitude decelerates with shear stress. Further, if the magnitude of the shear stress continues to increase, the maximum amplitude of the wave profile attenuates with shear stress and this phenomenon is displayed in figure 4(*b*). Again, the present result satisfactorily supports the result of primary instability, i.e. an increasing magnitude of

https://doi.org/10.1017/jfm.2014.351 Published online by Cambridge University Press

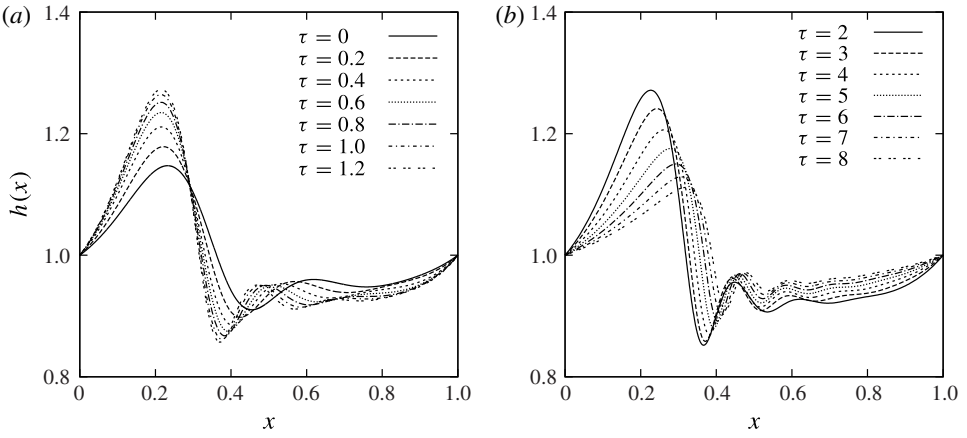


FIGURE 4. Travelling wave profiles corresponding to the low-dimensional model (3.3) and (3.9) for different values of shear stress in the downstream direction. Here $\theta = 90°$, $\Gamma = 253.0$, $k = 0.07$ and $Re = 5$.

imposed shear stress suppresses the transition process from primary flow to secondary flow.

In order to explore the mechanism of the smooth and continuous shape of the hump like travelling wave solutions, i.e. to figure out the reason why, physically, a travelling wave solution has a constant smooth shape without deformation for a particular wave speed, we first consider $We = O(\epsilon^{-1})$. Neglecting the second-order viscous dissipation terms, we are able to reduce (5.1) into the composition of kinematic and dynamic wave speeds

$$\tfrac{1}{7}Reh'(9 - h - h^2)(c - c_{d+})(c - c_{d-}) = \tfrac{5}{2}(h - 1)(c - c_k), \tag{5.6}$$

where

$$\begin{aligned} c_k &= \tfrac{1}{6}(2 + 3\tau + 2h + 3\tau h + 2h^2) \quad \text{with} \\ &\quad h = \tfrac{1}{4}\left(-2 - 3\tau \pm \sqrt{3}\sqrt{16c_k - 4 - 4\tau + 3\tau^2}\right), \end{aligned} \tag{5.7}$$

$$\begin{aligned} c_{d\pm} &= [(2 + 3\tau)(8h - 144) + 15\tau h^2 - 34\tau h^3] \pm Fr^2h^4\{2368Fr^2(2 + 3\tau)^2 \\ &\quad + 48h[10\,080 + 199Fr^2\tau(2 + 3\tau)] - h^2[53\,760 + Fr^2(2048\tau - 13\,569\tau^2)] \\ &\quad - h^3(53\,760 + 2844Fr^2\tau^2) - 668Fr^2h^4\tau^2\}^{1/2}/[96(h^2 + h - 9)]. \end{aligned} \tag{5.8}$$

Here c_k and $c_{d\pm}$ are respectively the kinematic and dynamic wave speeds associated with the nonlinear travelling waves. In general, each travelling wave develops from a primary neutral wave through a continuation process and propagates without any deformation with a particular speed for a particular Froude number or equivalently for a particular Reynolds number, and consequently such a wave can be considered as a secondary neutral wave. Thus, we must have $c_k = c_{d+} = c$ for a secondary neutral wave. This condition leads to an analytical expression for the speed of a family of travelling wave solutions as a function of the Froude number $c = c(Fr)$ not only in the drag–inertia regime (Ruyer-Quil & Manneville 2005; Samanta *et al.* 2011) but also in the drag–gravity regime. This speed is illustrated in figure 5 for different values of imposed shear stress. The present result is also verified by comparison with numerical

https://doi.org/10.1017/jfm.2014.351 Published online by Cambridge University Press

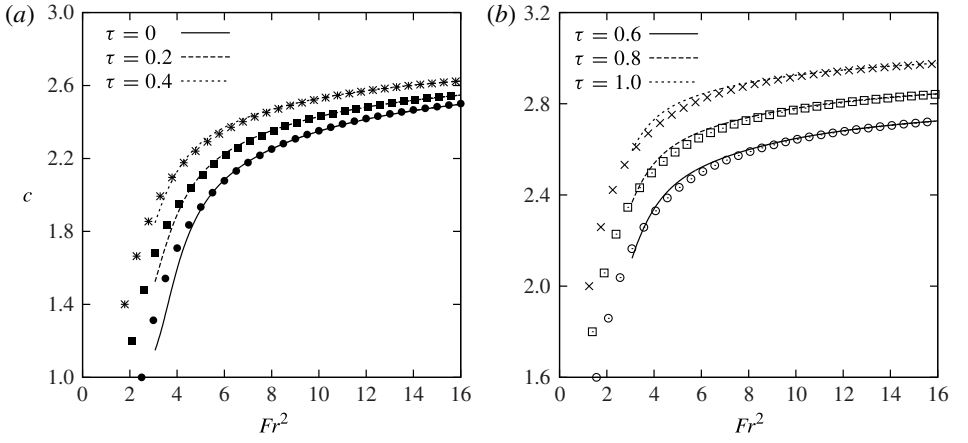


FIGURE 5. The variation of speed corresponding to the travelling wave solutions for different values of shear stress in the downstream direction. Here $\theta = 45°$ and $\Gamma = 6.0$. The solid lines represent the numerical results while the points denote the analytical results.

findings. For numerical experiment, we choose Rhodorsil silicone oil with kinematic viscosity $\mu/\rho = 50 \times 10^{-6}$ m^2 s^{-1}, $\sigma/\rho = 21.6 \times 10^{-6}$ m^3 s^{-2} and $\theta = 45°$ (Samanta *et al.* 2011) on account of the low magnitude of surface tension, which is neglected in the analytical derivation (5.6). Figure 5 shows the remarkable agreement between analytical and numerical results. A small discrepancy is detected in the transition zone between the drag–gravity and drag–inertia regimes (Ooshida 1999) because of the capillary term, which is absent from (5.6). In general, the drag–gravity regime means that viscous drag and gravitational force are dominant and inertia plays the role of perturbation; while the drag–inertia regime means that inertia is dominant. The new analytical result concludes that inertia force, viscous drag and streamwise gravitation force play a crucial role in the development of travelling wave solutions. The effect of capillary force is relevant only in the transition zone. Moreover, it is noted that the analytical result approaches the critical value of the Froude number $Fr_c^2 = 5/[2(1+\tau)]$ exactly at the neutral wave speed $c = 1 + \tau$ and this fact provides a link from the primary neutral wave to the secondary travelling wave solutions.

6. Direct numerical simulation

The spatiotemporal evolution of the low-dimensional model (3.3) and (3.9) for a shear-imposed falling film is performed by using a quasi-linearized Crank–Nicolson scheme (Richtmeyer & Morton 1967). The numerical scheme is consistent with second-order precision in time and the spatial derivatives are discretized by a central finite difference technique with second-order precision in space. Here we briefly describe the propose numerical scheme, which can also be found in detail in appendix F3 of the recent book by Kalliadasis *et al.* (2012). For convenience, the model (3.3) and (3.9) is written in matrix form

$$\partial_t \boldsymbol{U}(x, t) = \boldsymbol{M}(\boldsymbol{U}(x, t)), \tag{6.1}$$

where $\boldsymbol{U} = (h, q)^{\mathrm{T}}$ is a column matrix and the matrix $\boldsymbol{M}(\boldsymbol{U})$ contains all linear and nonlinear terms involving h, q and its spatial derivatives. First we discretize the

https://doi.org/10.1017/jfm.2014.351 Published online by Cambridge University Press

spatial and time domains into an equal space, i.e. $x_j = j\Delta x$ and $t_n = n\Delta t$, where $j, n = 1, 2, 3, \ldots$, Δx is the difference between two spatial grid points and Δt is the difference between two successive time steps. The variables h and q at the spatiotemporal grid point (x_j, t_n) are defined as h_j^n and q_j^n. Using the Crank–Nicolson scheme, the system (6.1) can be expressed as

$$\begin{aligned}(\boldsymbol{U}_j^{n+1} - \boldsymbol{U}_j^n)/\Delta t &= [\boldsymbol{M}(\boldsymbol{U}_j^{n+1}) + \boldsymbol{M}(\boldsymbol{U}_j^n)]/2 + O(\Delta t)^2 \\ &= [\boldsymbol{M}(\boldsymbol{U}_j^n + \Delta t \partial_t \boldsymbol{U}_j^n) + \boldsymbol{M}(\boldsymbol{U}_j^n)]/2 + O(\Delta t)^2 \\ &= \boldsymbol{M}(\boldsymbol{U}_j^n) + (\boldsymbol{U}_j^{n+1} - \boldsymbol{U}_j^n)\boldsymbol{M}'(\boldsymbol{U}_j^n)/2 + O(\Delta t)^2. \end{aligned} \tag{6.2}$$

The spatial derivatives that are involved in the algebraic system (6.2) are discretized by a central finite difference scheme and these derivatives are given by

$$\partial_x \boldsymbol{U}_j^n = (\boldsymbol{U}_{j+1}^n - \boldsymbol{U}_{j-1}^n)/(2\Delta x) + O(\Delta x)^2, \tag{6.3a}$$

$$\partial_{xx} \boldsymbol{U}_j^n = (\boldsymbol{U}_{j+1}^n - 2\boldsymbol{U}_j^n + \boldsymbol{U}_{j-1}^n)/\Delta x^2 + O(\Delta x)^2, \tag{6.3b}$$

$$\partial_{xxx} \boldsymbol{U}_j^n = (\boldsymbol{U}_{j+2}^n - 2\boldsymbol{U}_{j+1}^n + 2\boldsymbol{U}_{j-1}^n - \boldsymbol{U}_{j-2}^n)/(2\Delta x^3) + O(\Delta x)^2. \tag{6.3c}$$

In order to solve the algebraic system (6.2), the following upstream boundary condition is used:

$$\boldsymbol{U}(0, t) = (1, q(t))^{\mathrm{T}}. \tag{6.4}$$

However, downstream, we use a soft outlet boundary condition (Samanta *et al.* 2013) based on the lowest-order hyperbolic wave equation

$$\partial_t q + v_f \partial_x q = 0, \tag{6.5}$$

where $v_f > 0$ is the front velocity. This condition minimizes the generation of upstream-propagating disturbances and enhances numerical stability. The other initial condition is $\boldsymbol{U}(x, 0) = (h_0, q_0)^{\mathrm{T}}$, where $h_0 = 1$ and $q_0 = (1/3 + \tau/2)$. The water–glycerine mixture with density $\rho = 1070$ kg m^{-3}, kinematic viscosity $\mu/\rho = 6.27 \times 10^{-6}$ m^2 s^{-1} and surface tension $\sigma = 67 \times 10^{-3}$ N m^{-1} is selected for the present numerical experiment (Liu & Gollub 1994; Samanta 2013*a*; Samanta *et al.* 2013). A spatial response with a periodic harmonic forcing is applied at the inlet,

$$q(x, t) = q_0(1 + A\cos 2\pi ft), \tag{6.6}$$

where q_0 is the flow rate of the uniform liquid layer $h_0 = 1$, f is the frequency and A is the amplitude of the inlet forcing. Let us first consider the case when an imposed shear stress with magnitude τ acts in the downstream direction, i.e. $\tau > 0$. In order to justify the accuracy of a low-dimensional model, the present numerical results are also verified by comparison with the experimental observations (Liu & Gollub 1994) in the absence of imposed shear stress when the frequency of forcing alters successively. It is observed that when an imposed shear stress with magnitude $\tau = 1$ is applied at the free surface, the outcome of the nonlinear response corresponding to a forcing frequency $f = 7$ Hz evolves slowly downstream with increasing amplitude and eventually turns into a multi-peaked wave downstream with several humps. On the contrary, an initial small-amplitude perturbation simply turns into a sinusoidal-type periodic wave downstream in the absence of imposed shear stress. Such a scenario of the different character of wave profiles is displayed in figure 6. This result indicates that the presence of imposed shear stress is very sensitive to the spatial evolution of

https://doi.org/10.1017/jfm.2014.351 Published online by Cambridge University Press

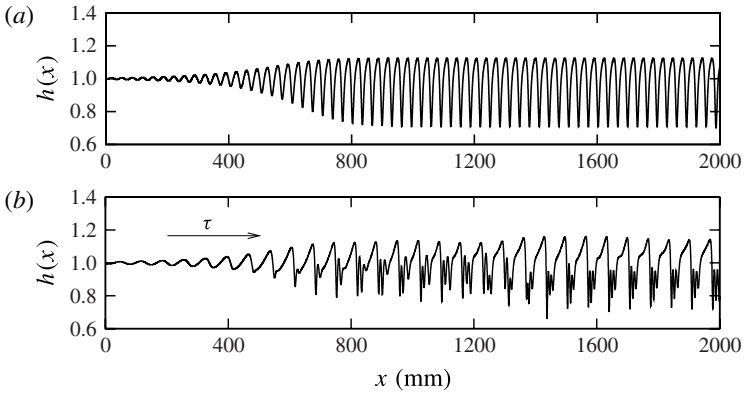


FIGURE 6. The spatial evolution of the inlet disturbance at large times with forcing frequency $f = 7$ Hz when $A = 0.01$, $\theta = 6.4°$, $Re = 58$ and $We = 35$: (*a*) $\tau = 0$ and (*b*) $\tau = 1$.

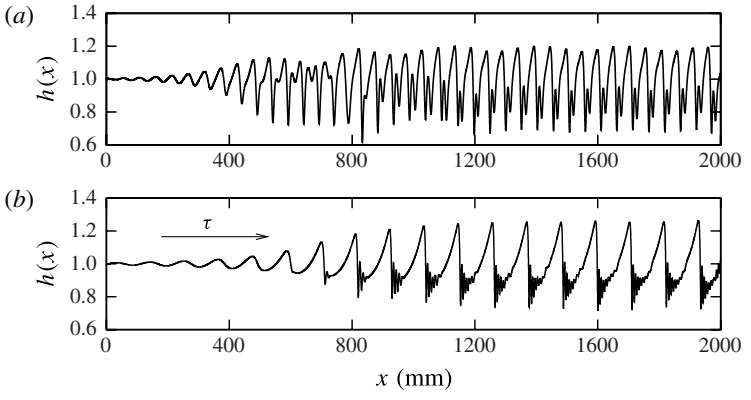


FIGURE 7. The spatial evolution of the inlet disturbance at large times with forcing frequency $f = 4.5$ Hz when $A = 0.01$, $\theta = 6.4°$, $Re = 58$ and $We = 35$: (*a*) $\tau = 0$ and (*b*) $\tau = 1$.

the initial disturbance and it qualitatively changes the structure of the wave profile downstream. Moreover, it makes faster the transition process of the spatially growing small-amplitude sinusoidal waves to multi-peaked waves. Further, in order to explore the behaviour of nonlinear responses at low frequency, another numerical experiment is carried out. However, only the applied forcing frequency is shifted from $f = 7$ Hz to $f = 4.5$ Hz; the other flow parameters are kept constant. The ensuing results are illustrated in figure 7. In this case, the small-amplitude sinusoidal waves undergo a transition to finite-amplitude localized pulses with a big hump preceded by capillary ripples. Further, the transition process becomes faster in comparison with the previous case. In addition, the amplitude of the localized pulses is larger than the amplitude of multi-peaked waves when we have a forcing frequency $f = 7$ Hz. Just after the inception region, the wave profile quickly develops into localized pulses with a large teardrop shape preceded by capillary ripples. On the other hand, if the imposed shear stress is removed, the transition process becomes somewhat slower than in the previous case and the resulting wave profile exhibits a multi-peaked wave phenomenon

https://doi.org/10.1017/jfm.2014.351 Published online by Cambridge University Press

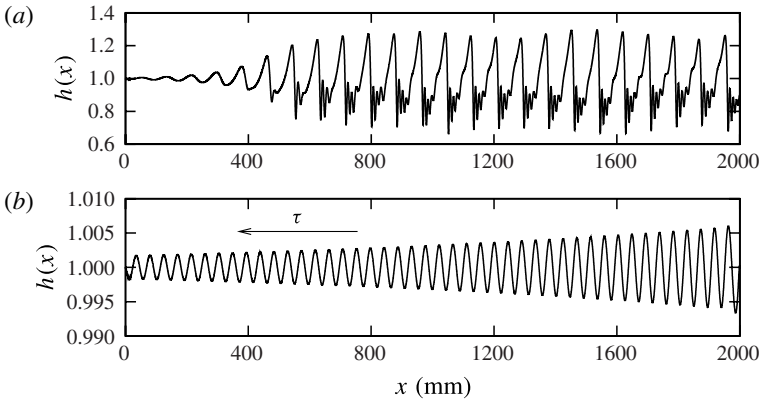


FIGURE 8. The spatial evolution of the inlet disturbance at large times with forcing frequency $f = 3$ Hz when $A = 0.01$, $\theta = 6.4°$, $Re = 58$ and $We = 35$: (*a*) $\tau = 0$ and (*b*) $\tau = -0.5$.

downstream. This fact was previously reported by Liu & Gollub (1994), Ruyer-Quil & Manneville (1998), Malamataris *et al.* (2002) and Samanta *et al.* (2013) in the context of a gravity-driven falling liquid film without shear.

Now we consider the case when the imposed shear stress acts in the upstream direction, i.e. $\tau < 0$. The numerical experiment is carried out by applying a forcing frequency $f = 3$ Hz when the magnitude of the imposed shear stress is kept constant at $\tau = -0.5$ and the flow parameters are retained the same as in previous numerical computations. The outcome of a nonlinear spatial response is demonstrated in figure 8. It is interesting to note that the application of an imposed shear stress in the upstream direction makes the wave amplitude weaker and turns them into a sinusoidal wave shape with an amplitude nearly equal to $A = 0.006$. On the other hand, without an imposed shear stress, one has localized shapes downstream with a big hump preceded by capillary ripples. Indeed, this result indicates that the presence of imposed shear stress in the upstream direction may delay the transition process from the small-amplitude sinusoidal waves to the finite-amplitude localized pulses with a big hump preceded by capillary ripples. In order to strengthen this physical issue, further another numerical test is performed where the forcing frequency is chosen as $f = 1.5$ Hz. The results can be found in figure 9. Again, a similar event occurs, i.e. the transition process from small-amplitude sinusoidal waves to finite-amplitude localized pulses with a big hump preceded by capillary ripples is weakened in the action of imposed shear stress in the upstream direction. However, in this case, the amplitude of the localized pulses is higher than in the previous case when we have a forcing frequency $f = 3$ Hz.

In order to examine the entire spatial evolution of the inlet disturbance downstream, we select a spatial domain approximately equal to 2000 mm. Consider an inlet forcing with a frequency $f = 3$ Hz. Further, we assume that the imposed shear stress acts in the downstream direction with magnitude $\tau = 1$. The ensuing result is depicted in figure 10. It is noticed that a regular train of solitary waves is generated far from the inception region corresponding to the forcing frequency $f = 3$ Hz and these waves travel almost with a same shape on the same substrate thickness. This fact specifies the saturation of waves downstream. The associated spatiotemporal diagram is displayed in figure 11, which also confirms the appearance of the regular pattern of solitary waves downstream.

https://doi.org/10.1017/jfm.2014.351 Published online by Cambridge University Press

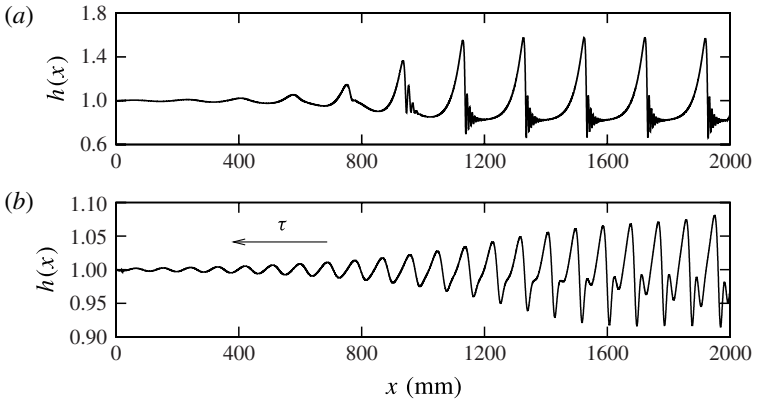


FIGURE 9. The spatial evolution of the inlet disturbance at large times with forcing frequency $f = 1.5$ Hz when $A = 0.01$, $\theta = 6.4°$, $Re = 58$ and $We = 35$: (*a*) $\tau = 0$ and (*b*) $\tau = -0.5$.

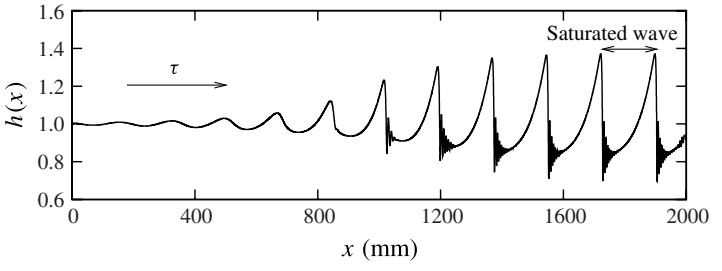


FIGURE 10. The spatial evolution of the inlet disturbance at large times with forcing frequency $f = 3$ Hz when $A = 0.01$, $\theta = 6.4°$, $Re = 58$, $We = 35$ and $\tau = 1$. See supplementary movie 1 available at http://dx.doi.org/10.1017/jfm.2014.351.

Further, in order to produce the result concerning the film falling down a vertical plane (Nosoko & Miyara 2004; Mudunuri & Balakotaiah 2006), we assume that the current film flow is preserved in the absence of imposed shear stress, i.e. $\tau = 0$. In what follows, we choose water with density $\rho = 998$ kg m^{-3}, kinematic viscosity $\mu/\rho = 1.004 \times 10^{-6}$ m^2 s^{-1} and surface tension $\sigma = 72.5 \times 10^{-3}$ N m^{-1} as the working liquid for this numerical experiment. Now we consider an inlet forcing with frequency $f = 14$ Hz. The resulting outcome of the nonlinear response is displayed in figure 12, which represents a regular train of solitary waves with a big hump preceded by capillary ripples after the inception region. The result satisfactorily agrees with the numerical result obtained by Nosoko & Miyara (2004) and Mudunuri & Balakotaiah (2006). Now we consider a noise-driven forcing at the inlet. This type of numerical simulation was provided by Chang, Demekhin & Kalaidin (1996), Chang, Demekhin & Sparikin (2002) and Samanta *et al.* (2013) in the context of a vertical falling film without shear. As a consequence, an irregular train of localized pulses with diversity in shape is developed downstream through a successive coalescence event where the larger pulses move faster and absorb the smaller ones during the entire transition process (Chang, Demekhin & Kalaidin 1995; Pradas, Tseluiko & Kalliadasis 2011). The complete scenario of the spatial evolution downstream corresponding to a noise-driven forcing is displayed in figure 13. Obviously, there are some situations

https://doi.org/10.1017/jfm.2014.351 Published online by Cambridge University Press

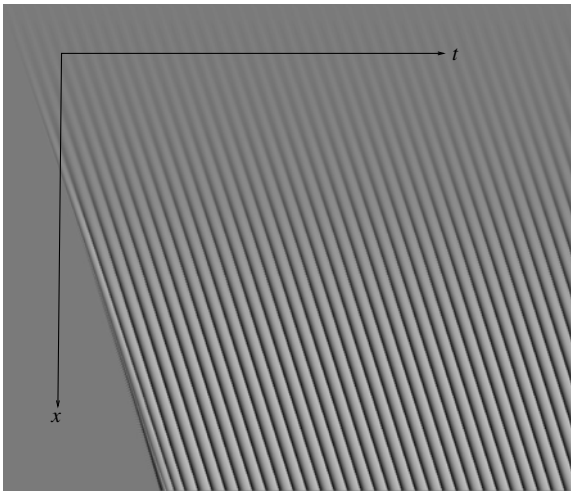


FIGURE 11. The spatiotemporal evolution of the inlet disturbance with forcing frequency $f = 3$ Hz when $A = 0.01$, $\theta = 6.4°$, $Re = 58$, $We = 35$ and $\tau = 1$.

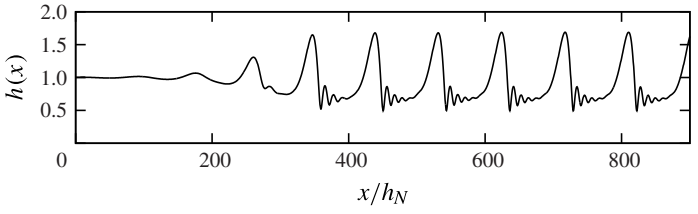


FIGURE 12. The spatial evolution of the inlet disturbance at large times with forcing frequency $f = 14$ Hz when $A = 0.01$, $\theta = 90°$, $Re = 48.3$, $We = 254.8$ and $\tau = 0$.

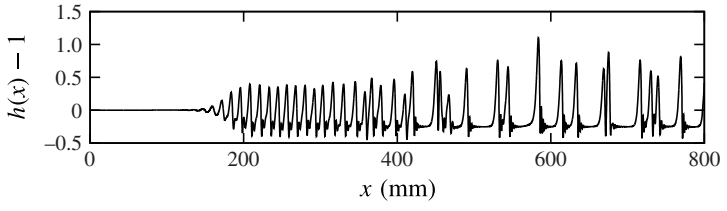


FIGURE 13. The spatial evolution of a noise-driven flow at large times when $\theta = 90°$, $\delta = Re/\kappa = 4.56$ and $\tau = 0$, where $\kappa = We^{1/3}$ is the Shkadov scale parameter (Shkadov 1967). See supplementary movie 2.

in figure 13 where two pulses are interacting with each other and finally evolve into a single big solitary pulse with time.

7. Conclusions

An alternative primary instability mechanism is provided for a gravity-driven falling film in the presence of imposed shear stress. Linear stability analysis of the low-dimensional model is performed under the framework of a two-wave structure,

https://doi.org/10.1017/jfm.2014.351 Published online by Cambridge University Press

which is normally a combination of kinematic and dynamic waves. It is revealed that the primary instability appears when the kinematic wave speed is faster than the speed of dynamic waves. An equality criterion between the kinematic and dynamic wave speeds yields the exact threshold of instability. Further, it demonstrates that the presence of imposed shear stress shows a destabilizing effect when its magnitude is rather low. If, further, the magnitude of the imposed shear stress continues to increase, a stabilizing influence is noticed. In general, the action of an imposed shear stress in the downstream direction promotes a base flow rate that is associated with the kinematic wave speed ($c_k = \mathrm{d}q/\mathrm{d}h|_{h=1}$, at $k \to 0$). Thus, the kinematic wave speed accelerates with the imposed shear stress. However, it decelerates with the viscous dispersion effect (see figure 2*a*). On the other hand, the dynamic wave speed c_{d+} accelerates with the viscous dispersion effect, and this effect completely vanishes at $k \to 0$. Accordingly, the imposed shear stress contributes to the long-wave instability by decreasing the critical Reynolds number. On the contrary, if the imposed shear stress acts in the upstream direction, the kinematic wave speed decelerates. Simultaneously, the dynamic wave speed also decelerates with a lower rate than the kinematic wave speed (see figure 2*b*). As a consequence, the gap between the kinematic and dynamic wave speeds enhances and this fact leads to a stabilizing effect on the primary instability.

In the nonlinear regime, it is noticed that, in the moving frame, the low-dimensional model can be reduced to a simple first-order ODE involving kinematic and dynamic wave speeds associated with the nonlinear travelling waves when the viscous dissipation and capillary effects are ignored (see (5.6)). As each travelling wave evolves from a primary neutral wave through a continuation process for a particular speed and particular Froude number, they may be considered as a secondary neutral wave. Consequently, an equality criterion between the kinematic and dynamic wave speeds yields an analytical expression for the speed of a family of travelling wave solutions as a function of the Froude number, not only in the drag–inertia regime, but also in the drag–gravity regime. Further, this analytical result is compared with the numerical finding for different values of imposed shear stress and an excellent agreement is achieved. The agreement between numerical and analytical results reveals that the inertial force, streamwise gravity and viscous drag force are essential in the development of travelling wave solutions. The effect of capillary force is relevant only in the transition zone between the drag–gravity and drag–inertia regimes. In addition, the present analytical result supplies a connection between the primary neutral wave and secondary travelling wave solutions, and this fact was not clarified previously.

Several time-dependent numerical simulations have been performed corresponding to the low-dimensional model in order to explore the spatiotemporal behaviour of nonlinear wave dynamics. It is found that the action of imposed shear stress in the downstream direction strengthens the transition process from small-amplitude periodic waves to finite-amplitude localized pulses with a big hump preceded by capillary ripples. On the contrary, the action of imposed shear stress in the opposite direction delays this transition process. The present numerical results are also verified with available numerical and experimental results in the absence of imposed shear stress, and satisfactory agreement is achieved.

Acknowledgements

This work is supported by the Inspire Faculty Award (IFA-13 ENG-44), Department of Science and Technology, Government of India. I would like to thank the reviewers

https://doi.org/10.1017/jfm.2014.351 Published online by Cambridge University Press

for their comments and suggestions to improve the manuscript. I am also grateful to Professor Christian Ruyer-Quil for insightful discussions on many occasions regarding this research topic.

Supplementary movies

Supplementary movies are available at http://dx.doi.org/10.1017/jfm.2014.351.

REFERENCES

ALEKSEENKO, S. V., NAKORYAKOV, V. Y. & POKUSAEV, B. G. 1985 Wave formation on a vertical falling liquid film. *AIChE J.* **31**, 1446–1460.

BENJAMIN, T. B. 1957 Wave formation in laminar flow down an inclined plane. *J. Fluid Mech.* **2**, 554–573.

BRAUNER, N. & MARON, D. M. 1982 Characteristics of inclined thin films, waviness and the associated mass transfer. *Intl J. Heat Mass Transfer* **25**, 99–110.

CHANG, H. C. 1994 Wave evolution on a falling film. *Annu. Rev. Fluid Mech.* **42**, 1553–1568.

CHANG, H. C., DEMEKHIN, E. A. & KALAIDIN, E. 1995 Interaction dynamics of a solitary waves on a falling film. *J. Fluid Mech.* **294**, 123–154.

CHANG, H. C., DEMEKHIN, E. A. & KALAIDIN, E. 1996 Simulation of noise driven wave dynamics on a falling film. *AIChE J.* **250**, 433–480.

CHANG, H. C., DEMEKHIN, E. A. & KOPELVITCH, D. I. 1993 Nonlinear evolution of waves on a vertically falling film. *J. Fluid Mech.* **250**, 433–480.

CHANG, H. C., DEMEKHIN, E. A. & SPARIKIN, S. S. 2002 Noise-driven wave transition on a vertically falling film. *J. Fluid Mech.* **462**, 253–283.

DOEDEL, E. J., CHAMPNEYS, A. R., FAIRGRIEVE, T. F., KUZNETSOV, Y. A., SANDSTEDE, B. & WANG, X.-J. 2007 Auto07: continuation and bifurcation software for ordinary differential equations. *Tech Rep*. Department of Computer Science, Concordia University, Montreal, Canada (available by FTP from ftp.cs.concordia.ca in directory pub/doedel/auto).

FINLAYSON, B. A. 1972 *The Method of Weighted Residuals and Variational Principles, with Application in Fluid Mechanics, Heat and Mass Transfer*. Academic Press.

GAO, D., MORLEY, N. & DHIR, V. 2003 Numerical simulation of wavy falling film flow using VOF method. *J. Comput. Phys.* **192**, 624–642.

KALLIADASIS, S., RUYER-QUIL, C., SCHEID, B. & VELARDE, M. G. 2012 *Falling Liquid Films*, 1st edn p. 205. Springer.

KAPITZA, P. L. 1948 Wave flow of thin layers of a viscous fluid: I. Free flow; and II. Fluid flow in the presence of continuous gas flow and heat transfer. In *Collected Papers of P. L. Kapitza (1965)* (ed. D. ter Haar), pp. 662–669. Pergamon.

KELLEY, R. E., GOUSSIS, D. A., LIN, S. P. & HSU, F. K. 1989 The mechanism for surface wave instability in film flow down an inclined plane. *Phys. Fluids* A **1**, 819–828.

LIU, J. & GOLLUB, J. P. 1994 Solitary wave dynamics of film flows. *Phys. Fluids* **6**, 1702–1712.

LIU, J., PAUL, J. D. & GOLLUB, J. P. 1993 Measurements of the primary instabilities of film flows. *J. Fluid Mech.* **250**, 69–101.

MALAMATARIS, N. A., VLACHOGIANNIS, M. & BONTOZOGLOU, V. 2002 Solitary waves on inclined films: flow structure and binary interactions. *Phys. Fluids* **14**, 1082–1094.

MUDUNURI, R. R. & BALAKOTAIAH, V. 2006 Solitary waves on thin falling films in the very low forcing frequency limit. *AIChE J.* **52**, 3995–4003.

NGUYEN, L. & BALAKOTAIAH, V. 2000 Modelling and experimental studies of wave evolution on free falling viscous films. *Phys. Fluids* **12**, 2236–2256.

NOSOKO, T. & MIYARA, A. 2004 The evolution and subsequent dynamics of waves on a vertically falling liquid film. *Phys. Fluids* **16**, 1118–1126.

OOSHIDA, T. 1999 Surface equation of falling film flows with moderate Reynolds number and large but finite Weber number. *Phys. Fluids* **11**, 3247–3269.

https://doi.org/10.1017/jfm.2014.351 Published online by Cambridge University Press

PRADAS, M., TSELUIKO, D. & KALLIADASIS, S. 2011 Rigorous coherent structure theory for falling liquid films: viscous dispersion effects on bound-state formation and self-organization. *Phys. Fluids* **23**, 044104.

RAMASWAMY, B., CHIPPADA, S. & JOO, S. W. 1996 A full-scale numerical study of interfacial instabilities in thin-film flows. *J. Fluid Mech.* **325**, 163–194.

RICHTMEYER, R. D. & MORTON, K. W. 1967 *Difference Methods for Initial Value Problems*. Interscience.

RUYER-QUIL, C. & MANNEVILLE, P. 1998 Modeling film flows down inclined planes. *Eur. Phys. J.* B **6**, 277–292.

RUYER-QUIL, C. & MANNEVILLE, P. 2000 Improved modeling of flows down inclined planes. *Eur. Phys. J.* B **15**, 357–369.

RUYER-QUIL, C. & MANNEVILLE, P. 2005 On the speed of solitary waves running down a vertical wall. *J. Fluid Mech.* **531**, 181–190.

SALAMON, T. R., ARMSTRONG, R. C. & BROWN, R. A. 1994 Traveling waves on vertical films: numerical analysis using the finite element method. *Phys. Fluids* **6**, 2202–2220.

SAMANTA, A. 2013*a* Effect of surfactant on two-layer channel flow. *J. Fluid Mech.* **735**, 519–552.

SAMANTA, A. 2013*b* Shear wave instability for a electrified falling film. *Phys. Rev.* E **88**, 053002.

SAMANTA, A., GOYEAU, B. & RUYER-QUIL, C. 2013 A falling film on a porous medium. *J. Fluid Mech.* **716**, 414–444.

SAMANTA, A., RUYER-QUIL, C. & GOYEAU, B. 2011 Falling film down a slippery inclined plane. *J. Fluid Mech.* **684**, 353–383.

SHKADOV, V. Y. 1967 Wave flow regimes of a thin layer of viscous fluid subject to gravity. *Izv. Akad. Nauk SSSR Mekh. Zhidk. Gaza* **1**, 43–51 (translation in 1970 *Fluid Dyn.* **2**, 29–34).

SMITH, M. K. 1982 The instability of sheared liquid layers. *J. Fluid Mech.* **121**, 187–206.

SMITH, M. K. 1990 The mechanism for the long-wave instability in thin liquid films. *J. Fluid Mech.* **217**, 469–485.

WEI, H. H. 2005*a* Effect of surfactant on the long-wave instability of a shear-imposed liquid flow down an inclined plane. *Phys. Fluids* **17**, 012103.

WEI, H. H. 2005*b* Stability of a viscoelastic falling film with surfactant subjected to an interfacial shear. *Phys. Rev.* E **71**, 066306.

WEI, H. H. 2007 Role of base flows on surfactant-driven interfacial instabilities. *Phys. Rev.* E **75**, 036306.

WEINSTEIN, S. J. & RUSCHAK, K. J. 2004 Coating flows. *Annu. Rev. Fluid Mech.* **36**, 29–53.

WHITHAM, G. B. 1974 *Linear and Nonlinear Waves*. p. 339. Wiley-Interscience.

YIH, C. S. 1963 Stability of liquid flow down an inclined plane. *Phys. Fluids* **6**, 321–334.

https://doi.org/10.1017/jfm.2014.351 Published online by Cambridge University Press